



Electrochemical machining process for micropit arrays using a rolling device with a linear cathode and a soft mask

Ge Qin¹ · Meng Li¹ · Lei Han¹ · Pingmei Ming¹ · Shen Niu¹ · Liang Yan¹ · Xingshuai Zheng¹ · Xinming Zhang¹ · Shiwei Li¹

Received: 10 May 2023 / Accepted: 16 July 2023 / Published online: 9 August 2023
© The Author(s), under exclusive licence to Springer-Verlag London Ltd., part of Springer Nature 2023

Abstract

Fabricating microstructure arrays on non-planar workpiece surfaces poses significant challenges. In this paper, we propose a novel electrochemical machining process for creating micropit arrays on such surfaces using a rolling device equipped with linear cathode and soft mask. This process employs a rotary electrochemical etching method to fabricate the microstructures, addressing the limitations of traditional mask electrochemical machining, such as the inability to achieve large-scale production and difficulties in preparing curved surfaces. A set of electrolytic systems with the rolling device was constructed to machine micropit arrays on various surfaces of the metal workpieces. Numerical simulations were conducted to investigate the evolution of the electric field distribution and the variation of micropit profiles over time in the machining area, and it was determined that electrolytic machining occurs only at the micropits closest to the linear cathode. When the ratio between the dimensions of the linear cathode and the mask hole is 1:3. Experimental tests were performed on the surface of a 304 stainless steel workpiece using a 10% NaNO₃ electrolyte and a 0.1 mm electrode gap. The results demonstrated that micropit arrays could be successfully machined on the plane, inner and outer surface of the workpiece. Under an applied voltage of 10.5 V and a workpiece rotating speed of 0.2 r/min, the diameter of the machined micropit was 421.55±18.75 μm, the depth was 70.2±4 μm, the average etch factor (EF) was 1.16, and the roughness of the micropit was 0.625±0.205 μm, which suggested that the machined micropit arrays have high precision and uniformity. These results indicate that the machined micropit arrays exhibit high precision and uniformity. This study presents a promising strategy for high-precision batch machining of micropit arrays on both planar and curved surfaces of workpieces.

Keywords Electrochemical machining · Rolling device · Linear cathode · Soft mask · Micropit arrays

1 Introduction

Fabricating microstructure arrays on metallic workpiece surfaces has gained significant interest in various fields, such as aerospace, bioengineering, and information technology engineering [1–3], due to the desirable surface characteristics it can provide, including improved friction reduction [4–7], heat dissipation [8, 9], wettability [1, 2, 10], and biocompatibility [3]. While several methods like micromilling, microelectric discharge machining, and laser machining can be employed for microstructure creation, they often result in undesirable effects such as burrs, residual internal stress,

microcracks, and deformations on the machined surface, negatively impacting the workpiece's properties and machining quality.

Electrochemical machining (ECM) is a process that utilizes electrochemical reactions to dissolve the metallic anode and remove material, resulting in specific shapes on the metal surface [11, 12]. ECM offers advantages by removing trace amounts of material through ion dissolution, eliminating tool loss, residual stresses and microdefects typically associated with mechanical cutting forces or hot-melt machining. Consequently, ECM has become increasingly popular in microfabrication. One ECM method, known as through-mask electrochemical micromachining (TMEMM), enables the creation of mm/sub-mm-sized structures on metallic workpieces [13, 14]. TMEMM employs masks to selectively machine microtexture arrays in designated areas, allowing for controllable structural shapes with high

✉ Ge Qin
qing512@163.com

¹ School of Mechanical and Power Engineering, Henan Polytechnic University, Jiaozuo 454000, Henan, China

productivity. Due to these benefits, TMEMM has become a promising and widely used technique for machining microstructures on metallic surfaces. However, the machining of micro and nanostructures using TMEMM often relies on photoresist masks, which protect non-machined regions during the lithography process [15, 16]. Unfortunately, these masks cannot be reused, requiring a separate mask for each process. Additionally, the limitations of this process currently restrict their usage to the flat workpieces, impeding its large-scale promotion and application. To address these limitations, Zhu et al. proposed the active mask electrochemical machining method, which mechanically attached a pre-prepared mask to the workpiece or tool without bonding, enabling mask reusability and reducing operating steps [17]. However, this technique still faces the limitations in the machining curved surfaces. To overcome this, Professor Ningsong Qu introduced polydimethylsiloxane (PDMS) material for active masks, improving machining accuracy [18]. And the authors of this paper proposed an ultra-flexible porous material-filled mask electrochemical machining and the foam cathode mask electrochemical machining techniques, effectively solving the challenge of attaching the active masks to the cylindrical workpieces [19, 20]. Nonetheless, these masks are suitable for specific-sized cylindrical workpieces and cannot be repeatedly used for processing the different sizes workpieces. Shen et al. proposed a method of continuous mask bulk processing, which is suitable for the batch continuous processing of cylindrical workpieces of any size, but the machining accuracy of the micropits in its contour is low ($EF=0.78$) [21]. Therefore, addressing the challenges of large-scale production and high-precision machining of the microstructures on the non-planar workpieces remains an important problem to be solved in TMEMM.

While TMEMM techniques simplify the machining process and increase efficiency and applicability, TMEMM using the traditional large-area cathode suffers from redundant electric current distribution in both machined and unmachined areas, resulting in poor microstructure

homogeneity and localization on the workpiece surface. The main reason for the low accuracy of the machined structure profile in TMEMM is the electric field distribution caused by the large cathode area, which affects both the machined and unmachined areas. Does reducing the size of the cathode decrease the impact of the electric field distribution on the machining area and improve machining precision? To investigate this, a novel ECM for machining micropit arrays that utilizes a rolling device with a linear cathode and a soft mask was proposed in this paper. A model was constructed to analyze the evolution process of the micropits and the electric distributions under different parameters. Furthermore, the proposed method was experimentally validated by machining the micropit arrays on the plane, inner, and outer cylindrical surfaces of the workpieces with optimized machining parameters.

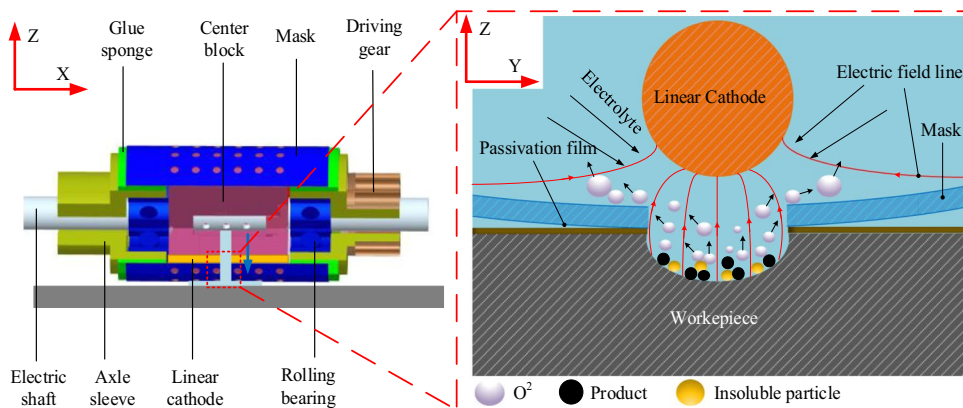
2 Method description and model analysis

To illustrate the principles of the proposed electrochemical machining, simulation analyses of the process using the linear cathode and the rolling mask are carried out. The current density distribution and the profile change law of micropits in this process are analyzed, and the effects of the linear cathode size on the electric field distribution have also been discussed. Additionally, the effects of the applied voltage and the linear cathode moving speed on the micropit profiles are investigated under the moving mask electrolysis conditions.

3 Method description

Figure 1 illustrates a rolling device that employs a linear cathode to machine micropit arrays in the electrochemical machining process. The rolling device features a hollow electric shaft at its center, onto which a flexible polyvinyl chloride (PVC) mask with rows of micro through-holes is

Fig. 1 The schematic diagram of rolling device with mask and linear cathode in the electrochemical machining process for micropit arrays



affixed to its outer surface. One end of the electric shaft is closed, while the other end is open, and there are some holes in the middle of the shaft. A center block is assembled on the middle of the electric shaft, which contains channels to allow for the electrolyte to flow, and is used to hold the linear cathode. Rolling bearings are attached to both sides of the center block on the electric shaft, and axle sleeves are fitted on the outer ring of the rolling bearings. Two pieces of glue sponges are adhered to the axle sleeves to hold the PVC mask in place. A gear is mounted on the axle sleeve to drive the rolling device. When power is transferred to the gear, it rotates and drives the axle sleeves, the outer ring of the rolling bearings and the mask, while the inner ring of the rolling bearings, the center block and the electric shaft remain stationary. The linear cathode, made of a copper wire, is assembled in a groove at the bottom of the center block to face the workpiece through the mask.

During the electrolytic machining process, the electrolyte is introduced into the electric shaft through the opening end and flows through the holes in the shaft and the channels in the center block. And then it fills the spaces between the center block and the mask and flows out between the mask and the workpiece. As the designed rolling device rotates, the center block and the linear cathode remain stationary while the mask and glue sponges rotate to drive the workpiece movement. Due to the mask, metal corrosion occurs only on the surfaces of the workpiece underneath the mask holes and the linear cathode (as shown in Fig. 1). The unique structural characteristics of the rolling device allow it to continuously roll on the workpiece, making it suitable for machining microstructured arrays on metal workpieces with the plane, inner, and outer cylindrical surfaces. A schematic diagram of the electrolytic machining process for workpieces with different surfaces using the designed rolling device is illustrated in Fig. 2.

4 Model built

During the electrochemical machining process, the dissolved region on the workpiece is mainly concentrated on the surface exposed in the through-holes of the mask and then the micropits arrays on the workpiece surface are formed with the rotating of the rolling device. In this paper, the entire machining process is simplified as the electrochemical machining between the cathode and anode in the machining area (as shown in Fig. 3).

The magnitude of current density in mask electrochemical machining can be obtained based on Ohm’s law and Faraday’s law:

$$i = \frac{\gamma(U - \delta E)}{\Delta} \tag{1}$$

where i is the current density, γ is the electrolytic conductivity, U is the applied voltage, δE is polarization potential, and Δ is the machining gap.

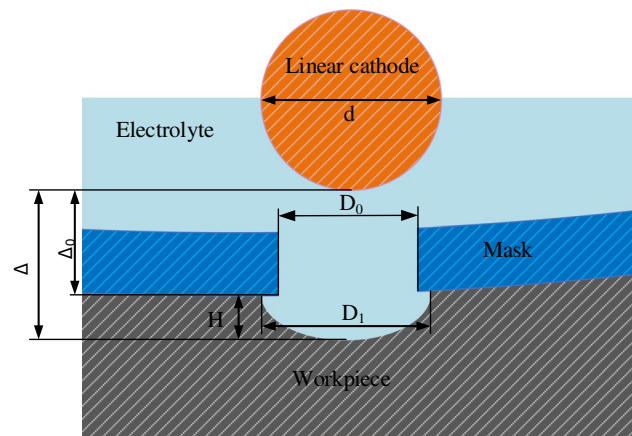


Fig. 3 The schematic of the electrochemical process using the linear cathode in the Y-Z plane

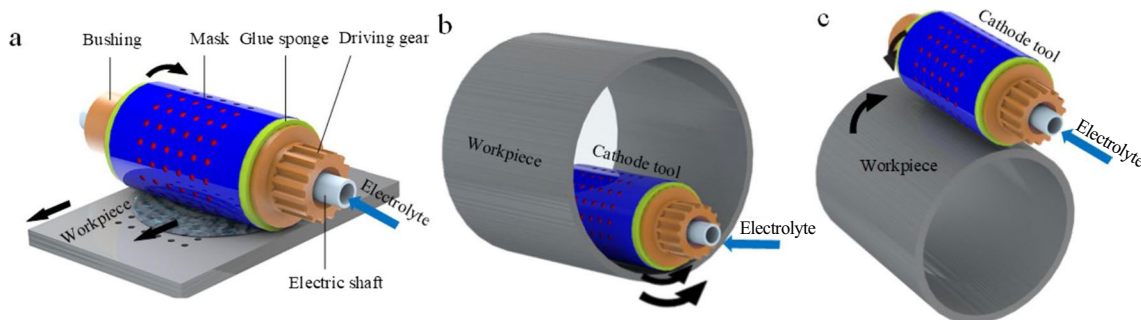


Fig. 2 Schematic diagram of the electrolytic machining process for the workpieces with different surfaces using the designed rolling device. a Plane workpiece; b inner cylindrical surface; c outer cylindrical surface

Therefore, the formula for anodic dissolution rate can be obtained based on Ohm’s law and current density:

$$V_a = \eta\omega i = \eta\omega \frac{\gamma(U - \delta E)}{\Delta} \tag{2}$$

where V_a is anodic dissolution rate and η is the current efficiency.

According to the above formula, when other conditions remain unchanged, the anodic dissolution rate of the anode workpiece is proportional to the voltage, current efficiency, electrochemical equivalent, and inversely proportional to the machining gap.

The machining gap (distance between the linear cathode and the workpiece) is Δ , the initial machining gap is Δ_0 , and after a period of time t of electrochemical machining, the depth of the micropits is H . The machining gap Δ when the machining time is t is as follows:

$$\Delta = \Delta_0 + H \tag{3}$$

Δ_0 is a constant set as the initial machining gap in the experiment. Differentiating the above formula, we can get

$$d\Delta = dH \tag{4}$$

Since $dH = v_a dt$ and combining with Equation (2), we know that $dH = [\eta\omega\gamma(U - \delta E)/\Delta]dt$. Therefore, we can derive

$$d\Delta = \eta\omega\gamma \frac{U - \delta E}{\Delta} dt \tag{5}$$

Integrating the above equation yields the relationship between machining gap and time t :

$$\Delta = \sqrt{2\eta\omega\gamma(U - \delta E)t + C} \tag{6}$$

Combining equations (3) and (6), which can obtain the formula for machining depth H and time t :

$$H = \sqrt{2\eta\omega\gamma(U - \delta E)t + C} - \Delta_0 \tag{7}$$

To analyze the evolution of the micropit profiles during the electrochemical machining process using the linear cathode, a simplified 2D model of both processes is established

Table 1 COMSOL simulation basic parameters table

Model parameters	Values
Anode boundary length per unit	0.3 mm
Cathode diameter	0.1~0.5 mm
Mask through-hole diameter	0.3 mm
Mask thickness	0.1 mm
Applied voltage	9~11 V
Initial conductivity of electrolyte	10 S/m
Initial temperature of electrolyte	25°C

in the Y-Z plane as shown in Fig. 4. Simulation parameters are provided in Table 1. In order to facilitate the simulation calculation, following assumptions are made:

- (1) The surfaces of the cathode and anode are equipotential, ignoring the effect of overpotential on the electrode surface potential.
- (2) The electric field, conductivity, and concentration are constant.
- (3) The electrolyte is a single-phase, incompressible, and continuous fluid.

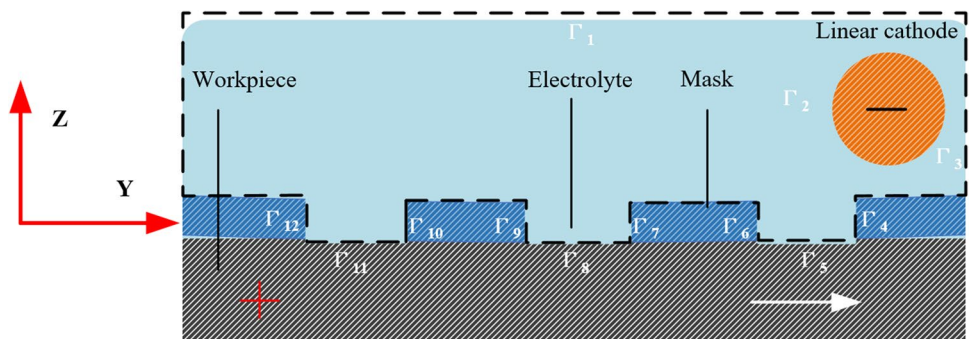
Based on the simplified two-dimensional geometric model of the electrochemical machining using a linear cathode and a mask, it can be inferred that the linear cathode, the workpiece anode, and the electrolytic cell together form a closed region Ω . Within the enclosed machining region, the current distribution follows the Laplace equation and can be mathematically described by the described by the following equation:

$$\nabla^2\phi = \frac{\partial^2\phi}{\partial x^2} + \frac{\partial^2\phi}{\partial y^2} = 0 \tag{8}$$

where x and y are the coordinates of points at the gap, ϕ represents the potential of the anode and the cathode, and ∇ represents the Laplace operator.

In this electrochemical machining process, the potential distribution of any point within the closed region Ω can be

Fig. 4 Schematic diagram of simplified two-dimensional model of conventional circular cathode and linear cathode mask electrochemical machining



determined using Equation (11), denoted as $\varphi(x, y)$. Additionally, the electric field intensity can be obtained by calculating the gradient vector distribution based on the potential distribution, as follows:

$$\nabla\varphi_e = -\frac{d\varphi}{dn}\vec{n} \tag{9}$$

where \vec{n} is the coordinate vector in a two-dimensional model, φ is the potential of the anode and cathode, and $\nabla\varphi_e$ is the electric field distribution at any point in the electrolytic cell.

The electrode surface can be treated as equipotential surface and the potential over the entire electrode is a constant. The boundary conditions for the cathode are described as follows:

$$\Gamma_2 = \varphi_2 = 0 \tag{10}$$

The electric field lines on the remaining boundaries are aligned with the direction of the normal vector of the boundary which is known as a closed boundary condition. And the boundary condition is described as a Neumann boundary condition which is set as follows:

$$\frac{\partial\varphi}{\partial n} \Big|_{\Gamma_{1,2,3,4,5,6,7,8,9,10,11,12}} = 0 \tag{11}$$

4.1 The results of solution

4.1.1 The influence of linear cathode size

In the electrochemical machining process, the size of the linear cathode can significantly affect the current density distribution within the machining area, resulting in varied micropit profiles. Figure 5 shows the corroded micropit profiles.

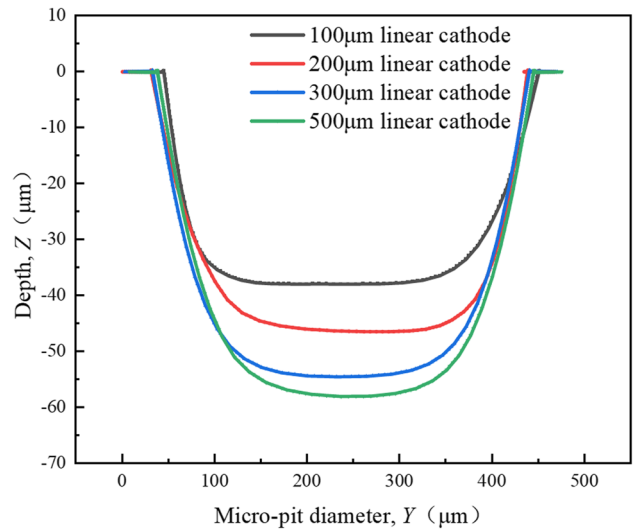


Fig. 6 The influence of linear cathode size on the profile of micropit 1

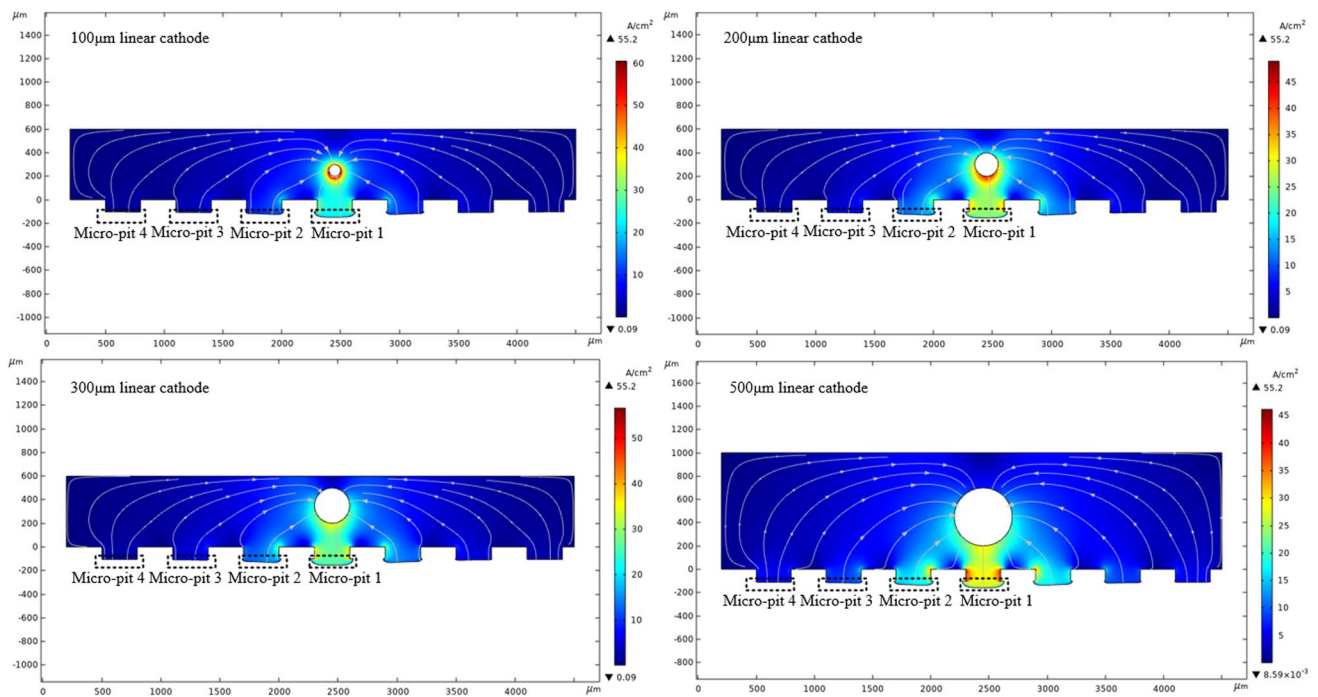


Fig. 5 Different linear cathode size mask electrolysis simulation current density distribution cloud diagram

sectional profile and the current density distribution cloud map on the machining area using linear cathodes with diameters of 100 μm , 200 μm , 300 μm , and 500 μm . Figure 6 displays the cross-sectional profile of micropit 1 in the Y-Z plane machined with different linear cathode sizes. When using a 100 μm diameter linear cathode, the micropit has the smallest depth and diameter with a depth-to-diameter ratio of 0.095. As the linear cathode diameter increases, the depth and diameter of the micropit gradually increase. When using a 300 μm diameter linear cathode, the diameter of the machined micropit does not increase significantly, but the depth and depth-to-diameter ratio increase significantly to 0.134. The profile of the micropit machined by the 500 μm diameter linear cathode is similar to that of the micropit electrolyzed using the 300 μm diameter linear cathode. The observed results may be attributed to the influence of the mask. When the ratio of the size of the linear cathode to the size of the mask hole is less than 1:1, the different electric field distribution in the corroded area leads to different diameters and depths of the resulting micropits. When the ratio is greater than 1:1, the electric field distribution in the corroded area tends to be consistent due to the shielding effect of the mask, but it begins to affect the electric field distribution of adjacent corroded areas. Figure 5 also shows that there are different electric field distributions in different micropits.

Figure 7 illustrates the current density distribution at the boundaries of micropits 2, 3, and 4, obtained using a linear cathode with diameter of 300 μm . It can be observed that the peak current density at the micropit 2, 3, and 4 is approximately 17 A/cm^2 , 8 A/cm^2 , and 5 A/cm^2 , respectively. The current density values at these micropits

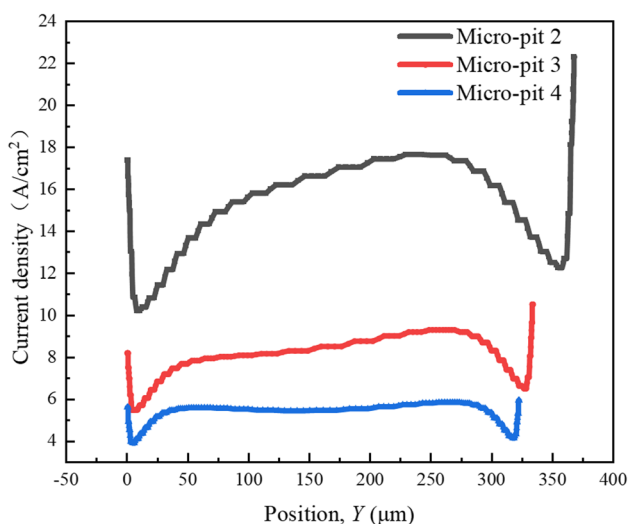


Fig. 7 The current density distribution of different micropits under 300 μm linear cathode electrolysis conditions

gradually decrease with the increasing of the distance between the micropit and the linear cathode. Previous studies have shown that electrolytic action on the surface can be considered negligible when the current density is less than 10 A/cm^2 in the electrochemical machining process [22]. Thus, only the surface directly below the linear cathode is corroded, and the surfaces at other locations remain uncorroded when the ratio of the mask hole and the space is 1:3. To minimize unnecessary etching of non-processing areas and previously processed areas by the linear cathode, it is recommended to increase the spacing between the mask holes. In the subsequent simulation, a spacing ratio of 1:3 between the mask holes arrays was used to achieve this goal.

4.1.2 Electrochemical machining process of the micropits

To investigate the formation mechanism of the micropits during the electrochemical machining process with linear cathode and rolling mask, the profile of the micropit 1 was simulated at different positions relative to the linear cathode with the movement of the workpiece, as shown in Fig. 8. Initially, the boundary of the micropit 1 was flat and without any etching. As the workpiece moves, the micropit 1 approaches the linear cathode, and the current density on the right side of the micropit becomes higher, causing etching to start at that position. As a result, the depth on the right side of the micropit 1 is greater than that on other positions. With the movement of the workpiece, the maximum current density moves in turn to the middle and left side of micropit 1. When the linear cathode is directly above micropit 2, the current density on the surface of the micropit 1 becomes too low to cause the electrochemical etching, resulting in the profile of the micropit 1 being corroded into an ideal symmetrical bowl shape. These results demonstrate that electrochemical corrosion occurs only when the linear cathode is located above or near the machined surface due to the smaller size of the linear cathode used, which is different from the traditional electrochemical machining process using large-area planar cathodes.

4.1.3 The influence of the workpiece moving speed

The current density distribution and the sectional profiles of the micropits at different moving speed of the workpiece are shown in Figs. 9 and 10, respectively. It can be observed that the depth of the micropits decreases significantly as the workpiece moving speed increases. When the moving speed of the workpiece was 100 $\mu\text{m}/\text{s}$, the etching depth of the micropits is the largest. This is because the machining

Fig. 8 Dynamic linear cathode mask electrochemical machining simulation process

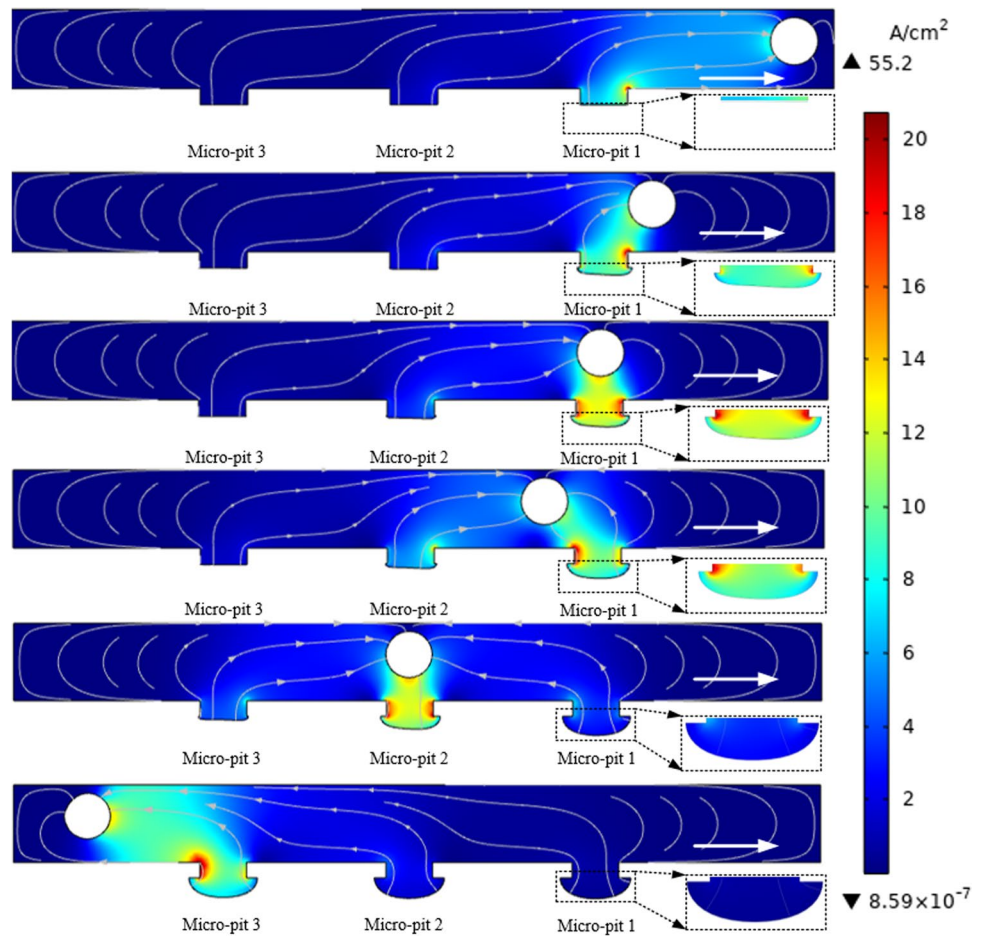
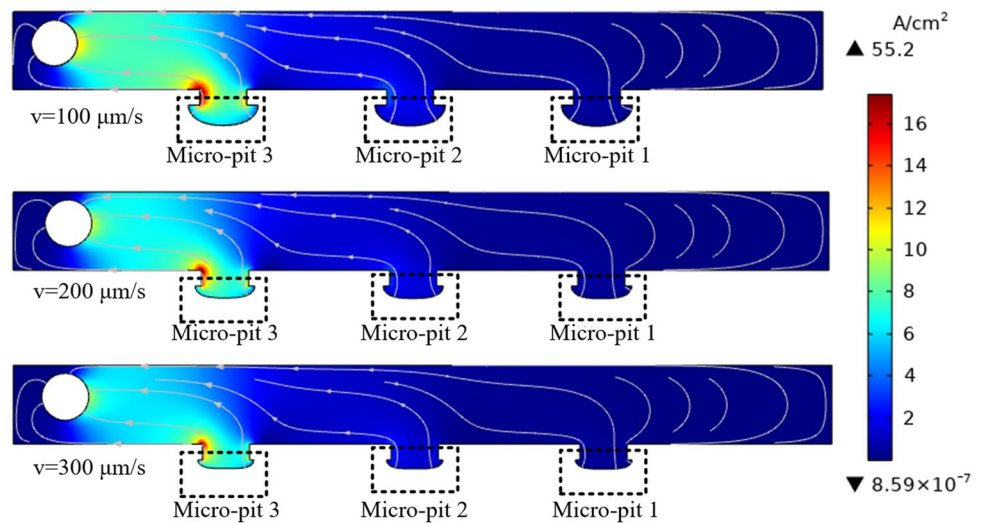


Fig. 9 Schematic diagram of the current density distribution diagram at different linear cathode speeds



time on the anode workpiece surface is longer at a slower moving speed, which results in a deeper etching depth of the micropits. Conversely, as the workpiece moving speed increases, the machining time becomes shorter, leading to a

smaller etching depth of the micropits. Thus, a small rotating speed of the rolling device can be selected in the experimental process to enhance the depth and the depth-to-diameter ratio of the micropits.

Fig. 10 Effect of linear cathode moving speed on micropit profile

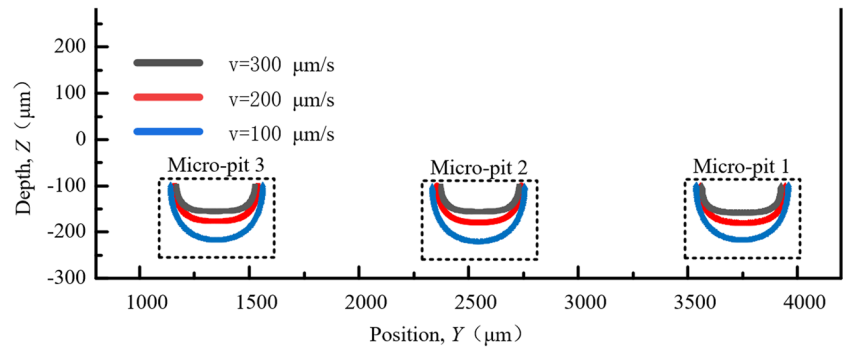


Fig. 11 Schematic diagram of the current density distribution diagram at different applied voltages

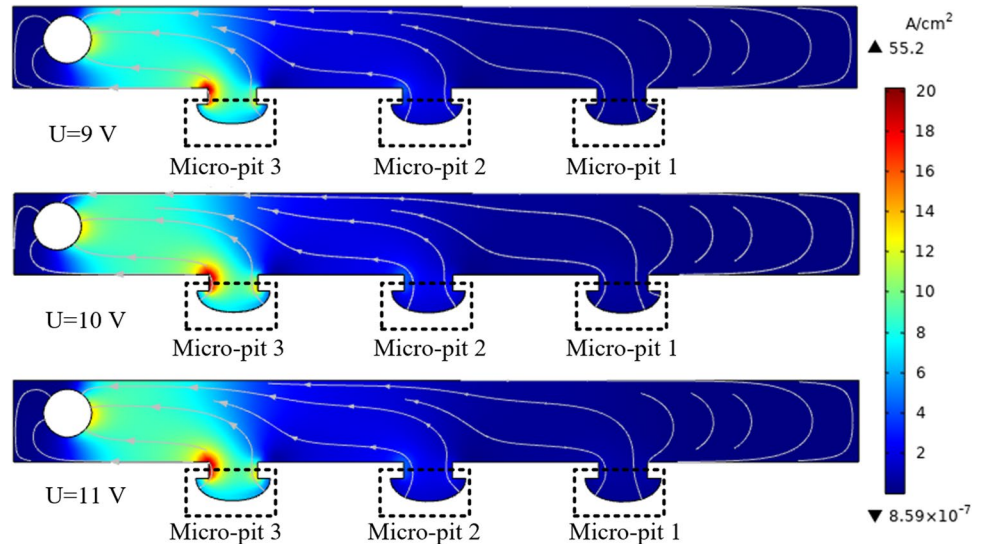
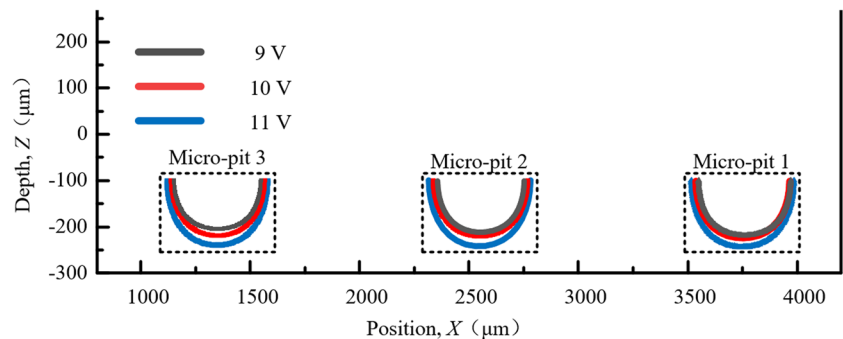


Fig. 12 The effect of applied voltage on the profile of micropits



4.1.4 The influence of the applied voltage

Figure 11 illustrates the current density distribution of the micropits machined under three different applied voltage conditions ($U=9$ V, 10 V, and 11 V). The sectional profiles of the micropits vary significantly with the applied voltage (as shown in Fig. 12). Specifically, as the applied voltage increases, the depth of micropits gradually increases. This phenomenon can be attributed to the higher current density generated between the workpiece and the linear cathode,

resulting in a more intense electrochemical reaction on the machined surface and a deeper etching depth of the micropits.

The above simulation results indicate that the electrochemical machining process using the designed rolling device with the linear cathode can improve the current distribution in the machining area by selecting appropriate sizes of the line cathodes and the spacing of the mask holes array. Moreover, the depth and localization of the microcavities can be enhanced by adjusting the moving speed of the workpiece and the applied voltage. These results demonstrate the

Fig. 13 Schematic diagram of the experimental system of linear cathode rolling printing electrochemical machining

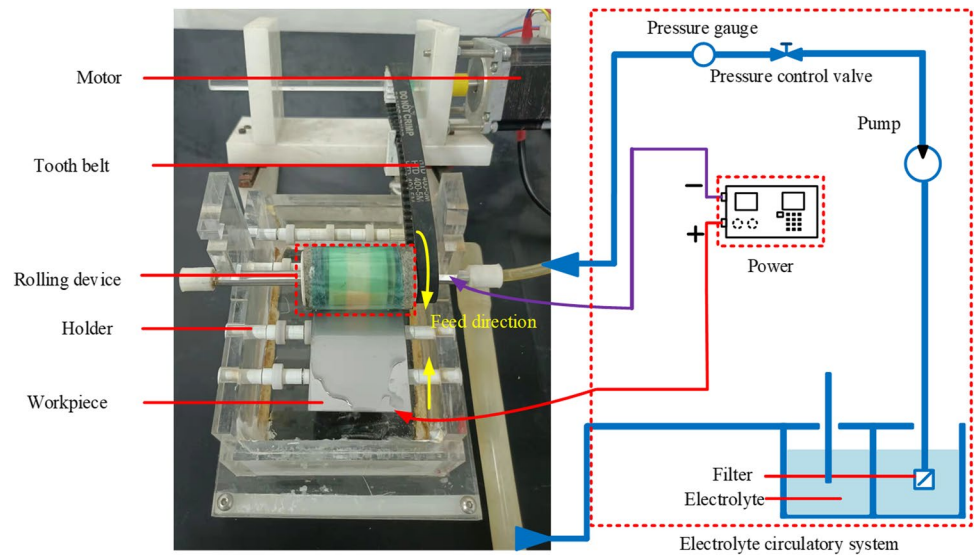


Table 2 Experimental parameters

Parameters	Value
Thickness of the mask	100 μm
304 stainless steel sheet	50 mm width ×5 mm thick
304 stainless steel tube	48 mm diameter ×5 mm thick
Material of linear cathode	Cu
Electrolyte concentration	10% (wt%), NaNO ₃
No-water ethanol concentration	98%
Applied voltage	9–12 V
Rotating speed of the mask	(0–0.5) r/min
Inter-electrode gap	0.1 mm
Electrolyte flow rate	1 L/min
Cathode tool diameter	35mm

potential of the proposed method for precise and efficient micromachining applications.

5 Experimental

The electrochemical machining process was carried out on a custom-built equipment, as shown in Fig. 13. The rolling device was mounted on a holder and connected to a gear fixed on the motor shaft via a tooth belt. A microhole array with a diameter of 300 μm and a spacing distance of 900 μm between the holes was fabricated on the mask using an ultra-precision CNC drill machine. The workpiece material utilized in the experiment was stainless steel 304, and NaNO₃ solution was employed as the electrolyte. The experimental parameters used are listed in Table 2.

The effects of process parameters on the morphology of micropit arrays were investigated using the designed device in the electrochemical experiments. The surface morphology of the workpiece was analyzed using an ultra-depth field microscope (VHX-2000, KEYENCE, Japan), a scanning electron microscope (SEM, Carl Zeiss NTS GmbH, Germany), and an Olympus microscope (Olympus LEXT OLS5000, Japan).

In this paper, the etching factor EF (Etch Factor) is used to describe the processing localization of the mask electrolysis process. Its expression is as follows:

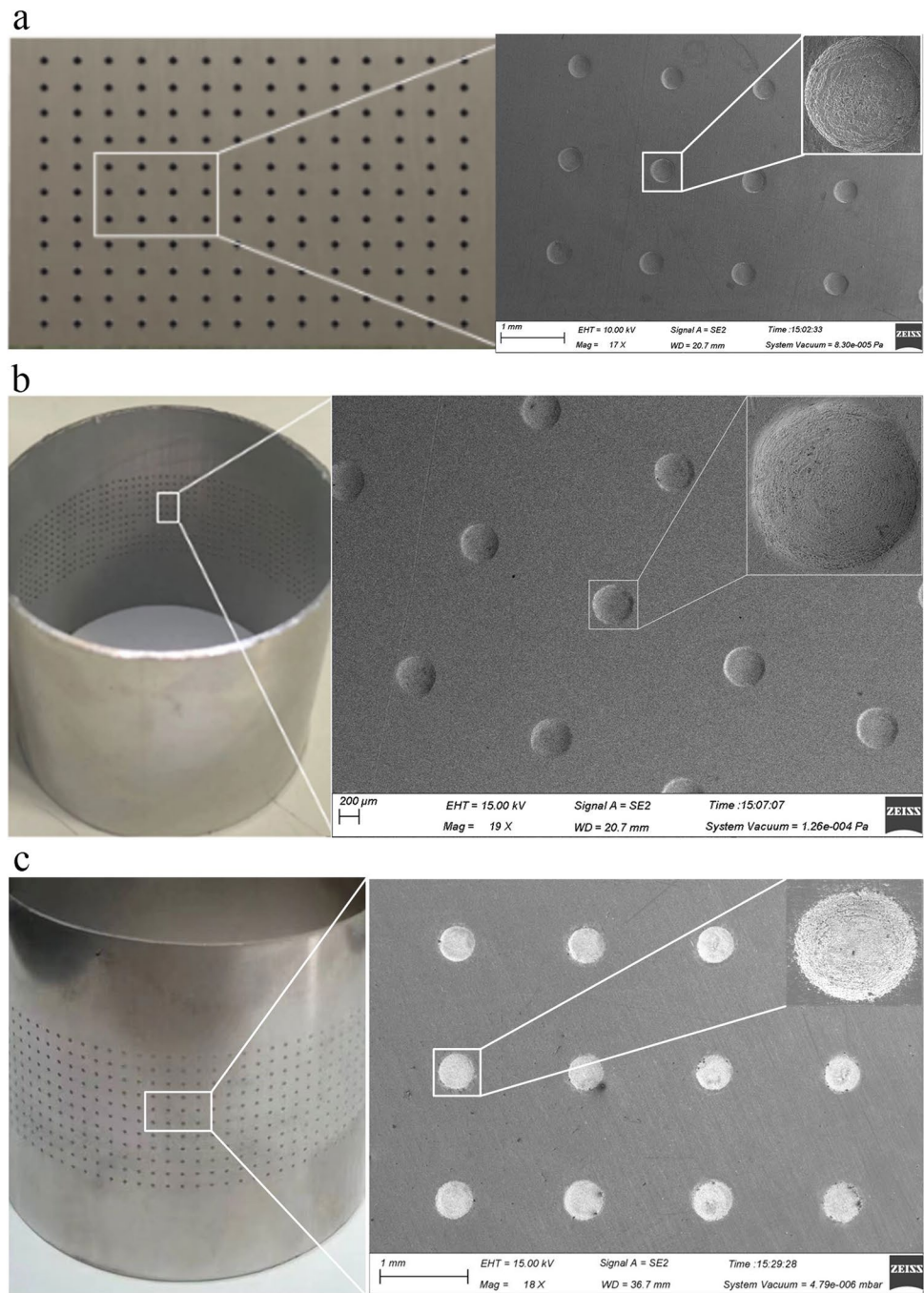
$$EF = h / (x_u - r_0) \tag{12}$$

where h is the micropit etching depth, x_u is the micropit etching radius, and r_0 is the mask hole radius.

6 Results and discussion

The electrochemical machining was carried out under the following conditions: a 10% (wt%) NaNO₃ electrolytic solution, the inter-electrode gap of 0.1 mm, the workpiece rotating speed of 0.2 r/min, and the applied voltage of 10.5 V. By using the designed device, the micropits with low roughness values and clear boundaries were obtained on the plane, inner and outer cylindrical surface of the workpiece. Figure 14 shows the morphology of the machined micropit arrays on the workpieces with these surface profiles, which demonstrated that the proposed method can achieve uniform micropit arrays on the plane, inner and outer surfaces of the workpiece. Figure 15 shows the profiles of the simulated and experimental micropit. The simulated micropit exhibited a

Fig. 14 Surface topography of the micropit arrays of the workpiece. **a** The flat workpiece; **b** the inner cylindrical workpiece; **c** the outer cylindrical workpiece



barrel-shaped profile, with a deeper etching depth and a smaller diameter, while the actual machined micropit presented a basin-shaped profile, featuring a shallower etching depth and a larger diameter. The primary cause of this difference lies in the limited consideration of electrolytic products and mass transfer effects during the simulation. In the actual electrochemical machining, as the machining time progresses, electrolytic products gradually accumulate within the micropits, impeding their timely removal and interfering with the ongoing

machining. Additionally, inadequate circulation and exchange of the electrolyte near the micropits further disrupt the machining process. These factors contribute to the results shown in Fig. 15.

To investigate the precision of the results, ten columns of the micropits were randomly selected and measured and analyzed the diameters and the roughness values of twenty micropits (two from each column), as shown in Fig. 16. The micropits obtained by the presented method exhibited a relatively concentrated size distribution, with

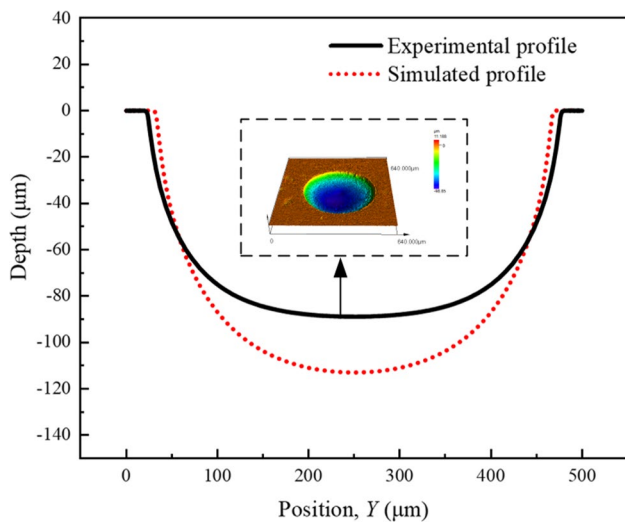


Fig. 15 The simulation and experimental profiles of the micropits

an average diameter of $421.55 \pm 18.75 \mu\text{m}$, a depth of $70.2 \pm 4 \mu\text{m}$, an average EF of 1.16, and a roughness of $0.625 \pm 0.205 \mu\text{m}$. The variances of the diameter, depth, and roughness of the micropits were $18.61 \mu\text{m}^2$, $2.53 \mu\text{m}^2$, and $0.0053 \mu\text{m}^2$, respectively. The results showed that the use of a linear cathode instead of the traditional large-sized cathode resulted in an increased EF from 0.78 to 1.16 [21], which suggested that the presented machining process of the micropit arrays had better localization.

7 Conclusions

To solve the challenge of the cost-effective electrochemical machining of a vast number of high-quality microstructures on the non-flat surface metal workpiece, a novel electrochemical machining using a rolling device with linear cathode and soft mask was proposed in this study. The theoretical model was developed built to analyze the evolution process of the micropits and the effect of the machining parameters. The feasibility of the proposed method had been verified through the experiments. Based on the theoretical analysis and the experimental results, the following conclusions were drawn:

- (1) The proposed rolling device enabled accurate profiling of micropits during the electrochemical machining process. By adjusting the diameters of the linear cathode and the spacing between the mask holes, the electric field distributions of the corroded surfaces could be modified. Notably, when the size ratio between the mask hole and linear cathode was 1:1 and the mask hole spacing exceeded 1:3, the current distribution concentrated only on the workpiece surface below the linear cathode. This resulted in the corrosion machining occurring exclusively in this location for smaller linear cathode sizes.
- (2) The experimental results demonstrated good agreement with the simulation, particularly regarding to the sectional profile of the micropits. The sectional profile of the micropits varied with different pro-

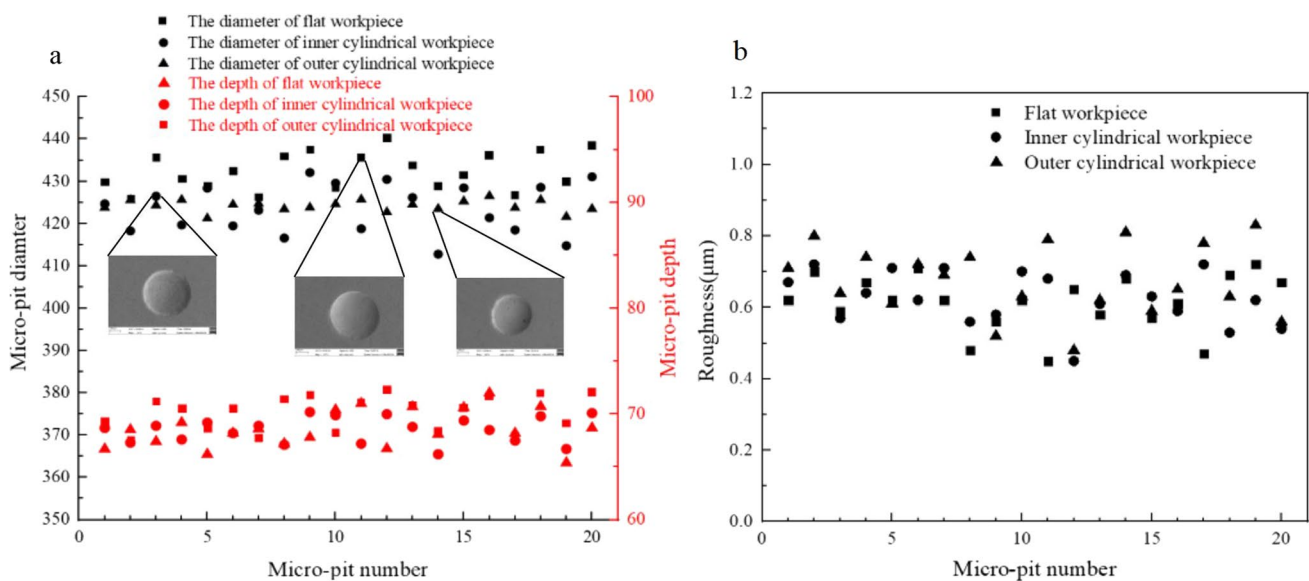


Fig. 16 Size and roughness distribution of micropit arrays of the planar workpiece: **a** the size distribution of micropit arrays; **b** the roughness distribution of micropit arrays

cessing voltages and rotating speeds of the workpiece. Under the electrolytic condition of 10.5 V processing voltage and 0.2 r/min rotating speed, a well-defined micropit array with smooth surfaces and clear edges was successfully fabricated.. Increasing the voltage and reducing of the rotating speed of the workpiece did not significantly alter the diameter of the micropits, but instead resulted in an increased depth of the micropits.

- (3) The proposed method allowed for the generation of micropit arrays on flat, inner, and outer cylindrical surfaces of the workpieces in a single step. The sectional profiles of the micropits exhibited an ideal bowl shape, with an average diameter of $421.55 \pm 18.75 \mu\text{m}$ and a depth of $70.2 \pm 4 \mu\text{m}$. The average EF was found to be 1.16, and the roughness of the micropits was $0.625 \pm 0.205 \mu\text{m}$. The variances of the diameter, depth, and roughness of the micropits were $18.61 \mu\text{m}^2$, $2.53 \mu\text{m}^2$, and $0.0053 \mu\text{m}^2$, respectively.

Author contributions Ge Qin: conceptualization, methodology, writing—original draft, writing—review and editing, visualization, and supervision. Meng Li: investigation, visualization, writing—review and editing, and conceptualization. Lei Han: investigation and writing—original draft. Pingmei Ming: investigation and writing—review and editing. Xinmin Zhang: investigation and resources. Shen Niu: resources, conceptualization, methodology, and writing—review and editing. Liang Yan: writing—review and editing, project administration, and conceptualization. Xingshuai Zheng: writing—review and editing, project administration, and conceptualization. Shiwei Li: writing—review and editing, conceptualization, supervision, and funding acquisition.

Funding This work is supported by the National Natural Science Foundation of China (No. 51105134), China Postdoctoral Science Foundation (No. 2020M682289), Key Research Development and Promotion Special Project (Science and Technology) of Henan Province (No. 232102221020), and Plan of Key Scientific Research Projects of Colleges and Universities in Henan Province (No. 21A460001).

Data availability Not applicable.

Code availability Not applicable.

Declarations

Ethics approval Not applicable.

Consent to participate Not applicable.

Consent for publication All authors have read and agreed to the published version of the manuscript.

Conflict of interest The authors declare no competing interests.

References

- Lu Y, Xu WJ, Song JL, Liu X, Xing YJ, Sun J (2012) Preparation of superhydrophobic titanium surfaces via electrochemical etching and fluorosilane modification. *J App Surf Sci* 263:297–301. <https://doi.org/10.1016/j.apsusc.2012.09.047>
- Song JL, Xu WJ, Liu X, Lu Y, Wei ZF, Wu LB (2012) Ultrafast fabrication of rough structures required by superhydrophobic surfaces on Al substrates using an immersion method. *Chem Eng J* 211:143–152. <https://doi.org/10.1016/j.cej.2012.09.094>
- Xu WJ, Zhao Y, Sun J, Hu K, Song JL (2013) Experimental study of super-hydrophobic surfaces obtained on steel matrix by brush plating technique. *J Chin Mech Eng* 24(1):5–9. <https://doi.org/10.3969/j.issn.1004-132X.2013.01.001>
- Hao XQ, Sun PC, Xiao SN, Yang YF, Li L (2020) Tribological performance of surface with different wettability under ball-on-disc test. *J Appl Surf Sci* 501:144228. <https://doi.org/10.1016/j.apsusc.2019.144228>
- Wang LL, Zhao XT, He MX, Zhang W (2021) Effect of micro grooves on lubrication performance of friction pairs. *J Meccanica* 56(2):351–364. <https://doi.org/10.1007/s11012-020-01295-y>
- Boidi G, Tertuliano IS, Profito FJ, de RW (2020) Effect of laser surface texturing on friction behaviour in elastohydrodynamically lubricated point contacts under different sliding-rolling conditions. *J Tribol Int* 149:105613–105613. <https://doi.org/10.1016/j.triboint.2019.02.021>
- Su BB, Huang LR, Huang W, Wang XL (2018) Observation on the deformation of dimpled surface in soft-EHL contacts. *J Tribol Int* 119:521–530. <https://doi.org/10.1016/j.triboint.2017.11.029>
- Cui XB, Li YH, Guo JX, Ming PM (2021) Effects of bio-inspired integration of laser-induced microstructure and coated cemented carbide on tool performance in green intermittent turning. *J Manuf Process* 65:228–244. <https://doi.org/10.1016/j.jmapro.2021.03.036>
- Cui XB, Li YH, Guo JX, Guo Q (2022) Transport behaviors and green interrupted cutting performance of bio-inspired microstructure on Al₂O₃/TiC composite ceramic surface. *J Manuf Process* 75:203–218. <https://doi.org/10.1016/j.jmapro.2022.01.002>
- Song JL, Huang WB, Liu JY, Liu H, Lu Y (2018) Electrochemical machining of superhydrophobic surfaces on mold steel substrates. *J Surf Coat Technol* 344:499–506. <https://doi.org/10.1016/j.surfcoat.2018.03.061>
- Zhan SD, Zhao YH (2020) Plasma-assisted electrochemical machining of microtools and microstructures. *Int J Mach Tools Manuf* 156:103596. <https://doi.org/10.1016/j.ijmactools.2020.103596>
- Wang J, Xu ZY, Wang JT, Xu ZL, Zhu D (2021) Electrochemical machining of blisk channels with rotations of the cathode and the workpiece. *Int J Mech Sci* 208:106655–106655. <https://doi.org/10.1016/j.ijmecsci.2021.106655>
- Zhai K, Du LQ, Wang SX, Wen YK, Liu JS (2020) Research on the synergistic effect of megasonic and particles in through mask electrochemical etching process. *J Electrochimica Acta* 364:137300–137300. <https://doi.org/10.1016/j.electacta.202037300>
- Chen XL, Fan GC, Lin CH, Dong BY, Guo ZN, Fang XL, Qu NS (2020) Investigation on the electrochemical machining of micro groove using masked porous cathode. *J Mater Process Technol* 276:116406–116406. <https://doi.org/10.1016/j.jmatprotec.2019.116406>
- Sun YK, Ling SY, Zhao DY (2020) Through-mask Electrochemical Micromachining of Micro Pillar Arrays on Aluminum. *J Surf Coat Technol* 401:126277–126277. <https://doi.org/10.1016/j.surfcoat.2020.126277>
- Wu M, Liu JW, He JF, Chen XL, Guo ZN (2020) Fabrication of surface microstructures by mask electrolyte jet machining. *Int J Mach Tools Manuf* 148:103471–103471. <https://doi.org/10.1016/j.ijmactools.2019.103471>

17. Zhu D, Qu NS, Li HS, Zeng YB, Li DL, Qian SQ (2009) Electrochemical micromachining of microstructures of micro hole and dimple array. *J CIRP Ann-Manuf Technol* 58(1):177–180. <https://doi.org/10.1016/j.cirp.2009.03.004>
18. Chen XL, Qu NS (2016) Li Hansong, Xu ZY (2016) Electrochemical micromachining of micro-dimple arrays using a polydimethylsiloxane (PDMS) mask. *J Mater Process Technol* 229:102–110. <https://doi.org/10.1016/j.jmatprotec.2015.09.008>
19. Ming PM, Zhou WH, Zhao CH, Zhou HM, Qin G (2016) Zhang XM (2016) Active through-mask electrochemical machining with its interelectrode gap filled with flexible porous material. *J Sci Sin Technol* 46(10):1005–1015. <https://doi.org/10.1007/s00170-017-0541-5>
20. Ming PM, Zhao CH, Zhang XM, Li XC, Ge Q, Yan L (2018) Investigation of foamed cathode through-mask electrochemical micromachining developed for uniform texturing on metallic cylindrical surface. *Int J Adv Manuf Technol* 96(9):3043–3056. <https://doi.org/10.1007/s00170-018-1755-x>
21. Shen JW, Ming PM, Zhang XM, Niu S, Xia YK, Zhang YY, Wang W, Li DD (2022) Fabrication of massive metal microstructures by rotating through-mask electrochemical transferring technology. *J Mech Eng* 58(11):295–307. <https://doi.org/10.3901/JME.2022.11.295>
22. Wang DY, Zhu ZW, Wang NF, Zhu D, Wang HR (2015) Investigation of the electrochemical dissolution behavior of Inconel 718 and 304 stainless steel at low current density in NaNO_3 solution. *Electrochim Acta* 2015(156):301–307. <https://doi.org/10.1016/j.electacta.2014.12.155>

Publisher's note Springer Nature remains neutral with regard to jurisdictional claims in published maps and institutional affiliations.

Springer Nature or its licensor (e.g. a society or other partner) holds exclusive rights to this article under a publishing agreement with the author(s) or other rightsholder(s); author self-archiving of the accepted manuscript version of this article is solely governed by the terms of such publishing agreement and applicable law.